Refined Solution Structure of 8,9-Dihydro-8-(N^7-guanyl)-9-hydroxyaflatoxin B_1 opposite CpA in the Complementary Strand of an Oligodeoxynucleotide Duplex As Determined by ^{1}H NMR†

David S. Johnston and Michael P. Stone*

Center in Molecular Toxicology and Department of Chemistry, Vanderbilt University, Nashville, Tennessee 37235

Received December 28, 1994; Revised Manuscript Received July 31, 1995®

ABSTRACT: The solution structure of d(CCATC^{AFB}GATCC)·d(GGATCAGATGG), containing the 8,9-dihydro-8-(N^7-guanyl)-9-hydroxyaflatoxin B_1 adduct, was refined using molecular dynamics restrained by NOE data obtained from ^{1}H NMR. The modified guanosine was positioned opposite cytosine, while the aflatoxin moiety was positioned opposite adenosine in the complementary strand. Sequential ^{1}H NOEs were interrupted between C^5 and $^{AFB}G^6$, but intrastrand NOEs were traced through the aflatoxin moiety, via H6a of aflatoxin and H8 of the modified guanine. Opposite the lesion, the NOE between A^{16} H1′ and G^{17} H8 was weak. A total of 43 NOEs were observed between DNA protons and aflatoxin protons. Molecular dynamics calculations restrained with 259 experimental and empirical distances, and using sp^2 hybridization at $^{AFB}G^6$ N7, refined structures with pairwise rms differences <0.85 Å, excluding terminal base pairs. Relaxation matrix calculations yielded a sixth root rms difference between refined structures and NOE intensity data of 7.3×10^{-2}. The aflatoxin moiety intercalated on the 5′-face of the modified guanine. The extra adenine A^{16} was inserted between base pair $^{AFB}G^6$·C^{15} and the aflatoxin moiety. A 36° bending between the plane of base pair $^{AFB}G^6$·C^{15} and the plane of the aflatoxin moiety was predicted. The aflatoxin moiety stacked below the top domain of the oligodeoxynucleotide, which consisted of base pairs C^1·G^{21}, C^2·G^{20}, A^3·T^{19}, T^4·A^{18}, and C^5·G^{17}. The bottom domain consisted of base pairs $^{AFB}G^6$·C^{15}, A^7·T^{14}, T^8·A^{13}, C^9·G^{12}, and C^{10}·G^{11}. The average winding angle between base pair C^5·G^{17}, the intercalated aflatoxin moiety, A^{16}, and base pair $^{AFB}G^6$·C^{15} was reduced to 10°. The preponderance of base pair substitutions in the aflatoxin B_1 mutational spectrum, particularly G → T transversions, suggests that the stability of this modified oligodeoxynucleotide, which models a templated +1 addition mutation, does not reliably predict the frequency of frame shifts.

Aflatoxin B_1 (AFB_1)[1] is the predominant mutagenic fungal metabolite isolated from several species of the genus *Aspergillus*. This mycotoxin is of worldwide health concern because of the potential contamination of the food supply. Epidermal absorption of AFB_1 from contaminated cosmetic products may also pose a risk (El-Dessouki, 1992). AFB_1 is a mutagen in several tester strains of bacteria (McCann et al., 1975), it is a hepatocarcinogen in experimental animals (Busby & Wogan, 1984; McMahon et al., 1990), and epidemiological studies suggest that it causes cancer in humans (Busby & Wogan, 1984; Groopman et al., 1988; Wogan, 1992). AFB_1 may be linked to site-specific transversions in the tumor suppression gene p53 (Bressac et al., 1991; Hsu et al., 1991) and *ras* protooncogenes (McMahon et al., 1990; Soman & Wogan, 1993).

AFB_1 is metabolized by specific cytochrome P_{450} enzymes (Shimada & Guengerich, 1989; Aoyama et al., 1990) to yield the ultimate carcinogen, AFB_1 *exo*-8,9-epoxide (Baertschi et al., 1988; Iyer & Harris, 1993) (Scheme 1). The *exo*-epoxide bonds predominate to the N7 position of guanine to yield *trans*-8,9-dihydro-8-(N^7-guanyl)-9-hydroxyaflatoxin B_1 (Essigmann et al., 1977). The regioselectivity of adduction is consistent with a mechanism whereby precovalent intercalation on the 5′-face of guanine (Stone et al., 1988, 1990; Gopalakrishnan et al., 1989a,b; Raney et al., 1990, 1993) places the epoxide in close proximity and in the proper orientation to the N7 position of guanine, thus facilitating a back-side S_N2 reaction (Iyer et al., 1994). AFB_1 prefers dsDNA by at least 1 order of magnitude over ssDNA; there also exists a strong preference for B-DNA over A-DNA with no detectable binding to Z-DNA (Raney et al., 1993). The isomeric aflatoxin B_1 *endo*-8,9-epoxide (Iyer & Harris, 1993) is not mutagenic and does not adduct DNA (Iyer et al., 1994), which further supports the existence of an intercalated transition-state complex with DNA.

^{1}H NMR studies of AFB_1−DNA adducts demonstrated that the aflatoxin moiety intercalated on the 5′-face of guanine (Gopalakrishnan et al., 1990). The related sterigmatocystin adduct was also intercalated (Gopalakrishnan et

† This work was supported by NIH Research Grant CA-55678 (M.P.S.) and NIH Instrumentation Grant RR-05805 (NMR spectrometer). Additional support for laboratory core facilities, including NMR spectroscopy, was provided by the Vanderbilt Center Grant in Molecular Toxicology, ES-00267. D.S.J. was supported by a training grant in Molecular Toxicology, ES-07028.

* Author to whom correspondence should be addressed.

® Abstract published in *Advance ACS Abstracts,* October 1, 1995.

[1] Abbreviations: AFB_1, aflatoxin B_1; DMT, dimethoxytrityl; DSS, sodium 4,4-dimethyl-4-silapentanesulfonate; EDTA, ethylenediaminetetraacetic acid; HPLC, high-pressure liquid chromatography; NOE, nuclear Overhauser enhancement; NOESY, two-dimensional nuclear Overhauser enhancement spectroscopy; PRP, polymeric reversed phase; ppm, parts per million; MD, molecular dynamics; MNDO, modified neglect of diatomic overlap; PEM, potential energy minimization; RMA, relaxation matrix; MD, molecular dynamics; rmsd, root mean square deviation; SCF, self-consistent field; TPPI, time-proportional phase increment; TOCSY, total homonuclear correlated spectroscopy; 1D, one dimensional; 2D, two dimensional.

0006-2960/95/0434-14037$09.00/0

Scheme 1. DNA Adduction by Aflatoxin B_1[a]

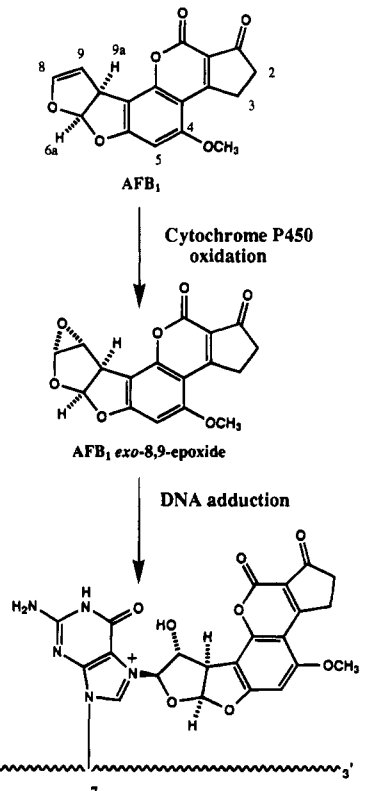

[a] AFB_1 is metabolized by cytochrome P_{450} enzymes to the ultimate carcinogen, aflatoxin B_1 8,9-*exo*-epoxide. This electrophile attacks the N7 position of guanine to form the 8,9-*trans*-dihydro-8-(N^7-guanyl)-9-hydroxyaflatoxin B_1 adduct.

al., 1992). The earlier work suggested that AFB_1 adduction should promote mutations at and 5′ to the lesion site. In the structures, the aflatoxin moiety was oriented such that the two keto oxygens might hydrogen bond with an incoming adenine or cytosine during replication. Alternatively, the aromatic adduct allowed for a potentially sizable stacking interaction with a purine.

The structural relationship between the aflatoxin moiety and an extra adenine nucleotide inserted into the complementary strand provides the basis for the present research. High-field NMR reveals that the oligodeoxynucleotide duplex d(CCATC^{AFB}GATCC)·d(GGATCAGATGG)[2] forms a stable structure in which both the AFB_1 moiety and the extra adenosine are intrahelical. Structural refinement, using a molecular dynamics/simulated annealing protocol restrained by NOE-based distances, shows that the AFB_1 moiety and the extra adenosine are partially stacked.

MATERIALS AND METHODS

AFB_1 was purchased from Sigma-Aldrich Chemicals, Inc. (Milwaukee, WI). Unadducted oligodeoxynucleotides were purchased from Midland Certified Reagent Co. (Midland, TX). Dimethyldioxirane was prepared (Murray & Jeyaraman, 1985) and reacted with AFB_1 to give the AFB_1 *exo*-8,9-epoxide (Baertschi et al., 1988). d(CCATC^{AFB}GATCC) was prepared as previously described for similar adducts (Gopalakrishnan et al., 1989b) and purified by HPLC using a PRP column (Hamilton, Inc., Reno, NV), equilibrated at 5 °C. It was eluted with a 20 min gradient from 5% to 25% v/v acetonitrile in a 5 mM sodium phosphate buffer (pH 6.8), with a flow rate of 1 mL/min (Gopalakrishnan et al., 1989b). The sample was desalted using Bio-Gel P-2 (Bio-Rad Laboratories, Richmond, CA) or Sephadex G-25 (Pharmacia-P.-L. Biochemicals, Piscataway, NJ). The adducted duplex was prepared by addition of an equal molar amount of the complementary strand d(GGATCAGATGG). Oligodeoxynucleotide concentrations were determined using the calculated UV extinction coefficients at 256 nm for d(CCATCGATCC), d(CCATC^{AFB}GATCC), and d(GGATCAGATGG) of 89.7, 102, and 115 × 10^{-3} M^{-1} cm^{-1}, respectively (Borer, 1975).

Spectroscopy. UV melting studies were performed in 0.01 M sodium phosphate buffer containing 1.0 M NaCl and 0.05 mM Na_2EDTA at pH 6.9. Melting data were collected in triplicate with a temperature rise of 1 °C/min. The temperature range was 5 → 80 °C. For NMR spectroscopy, the modified duplex was prepared at a concentration of ca. 250 A_{260} units/0.5 mL. For observation of nonexchangeable protons, the sample was dissolved in 0.5 mL of 0.01 M sodium phosphate buffer containing 0.1 M NaCl and 0.05 mM Na_2EDTA at pD 6.9. The sample was exchanged three times with 99.9% D_2O and dissolved in 99.96% D_2O. For observation of exchangeable protons, the D_2O was replaced with 9:1 H_2O−D_2O. Analytical HPLC chromatograms were obtained periodically to monitor sample integrity. Slow degradation (<0.25%/day) of the sample was observed over a 40 day period (the sample was kept at 5 °C or lower at all times). This was believed to be due to spontaneous depurination.

^1H NMR spectra were recorded at 500.13 MHz except for the T_1 relaxation experiments, which were recorded at 400.13 MHz. The temperature was controlled to ±0.5 °C. A phase-sensitive NOESY spectrum in D_2O, used for the assignments of the nonexchangeable protons, was recorded using a modified NOESY pulse sequence and the TPPI method for phase cycling. The NOESY pulse program was modified to eliminate artifacts arising from zero-quantum coherence and *zz* terms observed at short mixing times (Macura et al., 1982; Rance et al., 1985; Bodenhausen et al., 1984). The acquisition parameters were 1K real data points in the d_1 dimension with 32 acquisitions per FID, 2K real data points in the d_2 dimension, relaxation delay of 1.5 s, and a sweep width in both dimensions of 5051 Hz. The residual water resonance was saturated during the relaxation delay and the mixing period. T_1 relaxation experiments used the standard 180°−τ−90° inversion recovery sequence. Variable τ delays from 0.1 to 2.5 s were employed with 0.1 s increments. Sixteen transients were recorded per cycle × 40 cycles for a total of 640 transients/FID. Spectra in H_2O were obtained using a 1-1 binomial pulse sequence for water suppression (Plateau & Gueron, 1982; Hore, 1983). Two-dimensional phase-sensitive NOESY experiments in H_2O were carried out using a 1-1 sequence as the read pulse (Bax et al., 1987; Sklenar et al., 1987). Convolution difference

[2] The oligonucleotides discussed in this paper do not have terminal phosphate groups—we abbreviate the nomenclature for oligonucleotides by leaving out the phosphodiester linkage. A, C, G, T, and X refer to mononucleotide units. A superscript to the right refers to the numerical position in the oligonucleotide sequence starting from the 5′-terminus of chain A and proceeding to the 3′-terminus of chain A and then from the 5′-terminus of chain B to the 3′-terminus of chain B. C2, C5, C6, C8, C1′, C2′, C2″, etc. represent specific carbon nuclei. H2, H5, H6, H8, H1′, H2′, H2″, etc. represent the protons attached to these carbons.

Scheme 2. Experimental Design for the Adduction of Aflatoxin B_1 8,9-*exo*-Epoxide to N7 of G^6 [a]

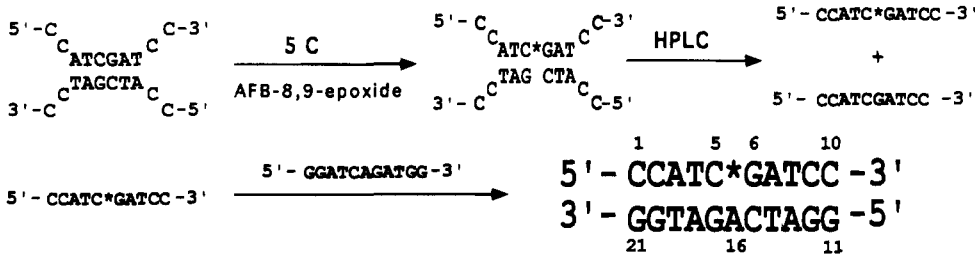

[a] The final duplex shows the numbering scheme for the subsequent NMR studies.

was used during processing to minimize the residual signal arising from water (Marion et al., 1989). Chemical shifts were referenced internally to the H_2O frequency. Data processing utilized FELIX 2.3 (Biosym Technologies, Inc., San Diego, CA), running on Iris workstations (Silicon Graphics, Inc., Mountain View, CA). A skewed sine-squared apodization of the NOESY data was used as the window function, such that the first point of the FID was multiplied by unity for an accurate determination of cross-peak volumes. Baseline correction utilized a fifth order polynomial.

Starting Structures. A-DNA (Arnott & Hukins, 1972) and B-DNA (Arnott & Hukins, 1972, 1973) starting structures were built with INSIGHTII (Biosym Technologies, Inc., San Diego, CA). AFB_1 was intercalated above the 5′-face of G^6, and a covalent bond was created between C8 of AFB_1 and N7 of G^6. Interatomic distances and bond angles for the AFB_1 atoms were obtained from the crystal structure (Van Soest & Peerdeman, 1970). The partial charges on AFB_1 were determined on the modified base using a charge of +1 for the adduct, from SCF calculations using MOPAC (Stewart, 1983) via the MNDO method. The guanine N7 was assumed to have sp^2 hybridization. The A- and B-DNA structures were minimized by the conjugate gradient method for 200 iterations without experimental restraints to give the starting structures IniA and IniB for subsequent RMA and MD calculations.

Distance Measurements. NOESY spectra measured at mixing times of 150, 250, and 350 ms were acquired. Footprint boxes were selected manually with FELIX 2.3 to fit well-resolved peaks at a contour level which showed the weak NOEs but not the spectral noise. Overlapped peaks were not used, except for the A^{16} H2 cross-peaks with AFB H2α, H3α, and H3β. A larger error was assigned to these distances. For each of the three mixing times, a hybrid intensity matrix was constructed using MARDIGRAS (Borgias & James, 1990), which consisted of experimental intensities supplemented with calculated intensities from IniB. RMA using CORMA (Keepers & James, 1984) yielded internuclear distances. Isotropic tumbling with τ_c of 6 ns was assumed. The methyl jump model 3 accounted for the rapid spin of the methyl groups (James, 1991).

Experimental distances were divided into three categories on the basis of standard deviations obtained from MARDIGRAS. A total of 190 high-quality, 33 medium-quality, and 13 low-quality distances were determined, for a total of 236 distance constraints. An additional 23 constraints were determined from the NOESY spectrum measured in H_2O buffer. These are tabulated in Tables 4S−7S in the supporting information. Larger error bounds were allowed for the latter distances since they were qualitatively classified as long, medium, and short range by visual inspection of the NMR data.

Restrained Molecular Dynamics. A detailed description is found in the supporting information. All calculations used X-PLOR (Brunger, 1992). The empirical energy function derived from CHARMM (Brooks et al., 1983) treated hydrogens explicitly (Nilsson & Karplus, 1986). The electrostatic term used the Coulombic function based on a reduced charge set of partial charges and a distance-dependent dielectric constant of 4.0. The van der Waals term used the Lennard-Jones potential energy function. The nonbonded pair list was updated if any atom moved more than 0.5 Å, and the cutoff radius for nonbonded interactions was 11 Å. All calculations were run *in vacuo* without explicit counterions. The effective energy function was comprised of terms describing distance and dihedral restraints, both of which were standard square well potentials (Clore et al., 1986).

Bond lengths involving hydrogens were fixed with the SHAKE algorithm (Ryckaert et al., 1977). Empirical base-pairing distance and planarity restraints were included. Torsion angle restraints were used to prevent excessive propeller twisting of Watson−Crick base pairs. Backbone torsion angles were restrained during high-temperature dynamics. For $d(C^1C^2A^3T^4)\cdot d(A^{18}T^{19}G^{20}G^{21})$ and $d(A^7T^8C^9C^{10})\cdot d(G^{11}G^{12}A^{13}T^{14})$, torsion angles were restricted to ranges which would sample both A- and B-DNA. At $d(C^{5AFB}G^6)\cdot d(C^{15}A^{16}G^{17})$ the 90% confidence interval was measured for the family of torsion angles emergent from 12 MD simulations performed without torsion restraints. Torsion ranges equal to twice the 90% confidence interval were added as restraints to calculations. Force constants for the $d(C^{5AFB}G^6)\cdot d(C^{15}A^{16}G^{17})$ torsion angles were half the magnitude of those used elsewhere in the molecule. The molecules were weakly coupled to a temperature bath with a coupling constant of 0.05 ps (Berendsen et al., 1984). The time step of the integrator was 1 fs. Structure coordinates were archived every 0.1 ps over the final 15 ps. The emergent structures were averaged over the last 5 ps of the MD calculations. Convergence was monitored by calculating pairwise rmsd for final structures. Accuracy was assessed by RMA using CORMA. The refined structures were analyzed using DIALS AND WINDOWS 1.0 (Ravishankar et al., 1989). The helicoidal analysis was performed separately for the two fully base-paired regions of the molecule, while parameters for the unpaired adenine were recorded manually using INSIGHTII for graphical display.

RESULTS

Adduct Synthesis. The synthetic strategy for obtaining the adducted duplex is shown in Scheme 2. Aflatoxin B_1 *exo*-

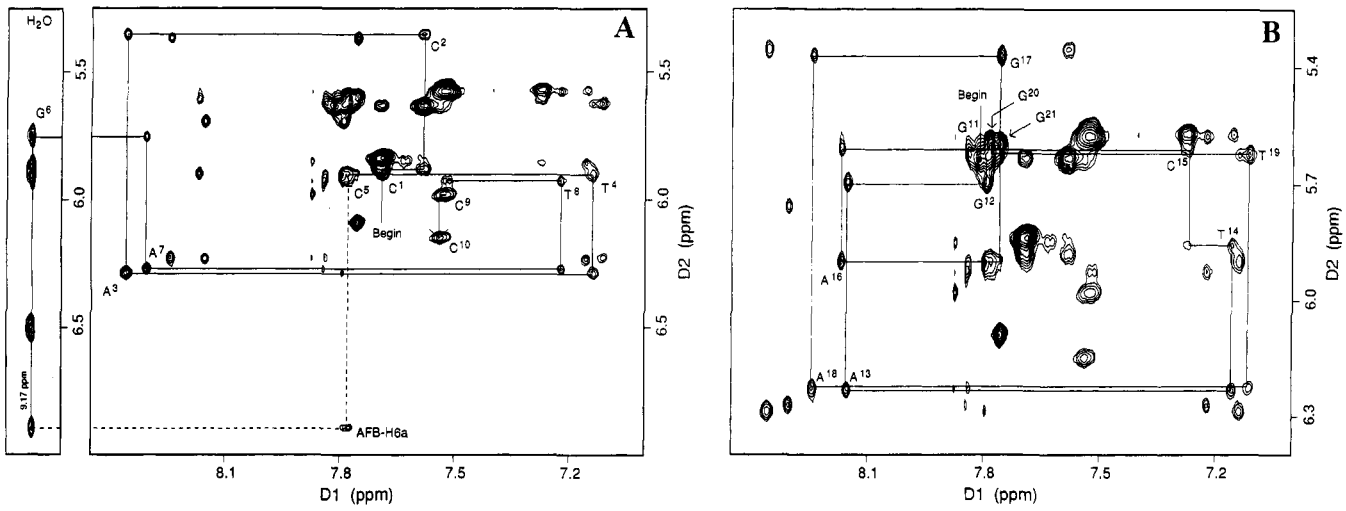

FIGURE 1: Sequential NOE connectivities observed for (A) the adducted strand and (B) the unadducted strand at pD 6.9.

8,9-epoxide was reacted with the homoduplex d(CCATCGATCC)$_2$, which was assumed to form a B-form hexameric duplex with overhanging cytosine at both the 5′- and 3′-ends (T_m = 26 °C). Whether the latter assumption was correct was not determined; however, the reaction produced the desired product, d(CCATC^{AFB}GATCC).[3] This prevented formation of regioisomeric adducts which might have been formed had the epoxide been reacted directly with d(CCATCGATCC)·d(GGATCGATGG), the fully complementary duplex, in which two G·C base pairs were located at each end of the duplex. The adducted and nonadducted strands were separated by reverse-phase HPLC after which an equimolar aliquot of the complement 5′-d(GGATCAGATGG)-3′ containing an extra adenine opposite aflatoxin was added.

Adduct Stability. The results of a series of UV melting profiles for d(CCATCGATCC)·d(GGATCGATGG) and related oligodeoxynucleotides demonstrated that the aflatoxin adduct stabilized the extra adenine located in the complementary strand of the duplex. In the melting studies, DNA strand concentration was maintained at ~5 μM. For the fully complementary parent duplex d(CCATCGATCC)·d(GGATCGATGG), a melting temperature of 52.0 °C was observed. Formation of the modified duplex d(CCATC^{AFB}GATCC)·d(GGATCGATGG) increased the melting temperature to 53.0 °C, similar to d(ATC^{AFB}GAT)·d(ATCGAT) (Gopalakrishnan et al., 1989b). When an additional adenine was inserted into the complementary strand, forming the unmodified duplex d(CCATCGATCC)·d(GGATCAGATGG), the melting temperature was reduced to 39 °C. Addition of the aflatoxin adduct resulted in thermodynamic stabilization; the T_m of d(CCATCA^{AFB}GATCC)·d(GGATCAGATGG) was 45.5 °C. The UV melting temperature of this duplex was examined as a function of pH. Comparison of the data at pH 6.1 with that at pH 7.1 revealed that the T_m of d(CCATCA^{AFB}GATCC)·d(GGATCAGATGG) was increased from 45.5 to 49.0 °C at the lower pH value. When an A·T base pair was inserted between the cental G·C base pairs, the T_m of d(CCATCTGATCC)·d(GGATCAGATGG) was determined to be 52.0 °C. A plot of the melting data is shown in Figure 2S in the supporting information.

NMR Spectroscopy. (a) DNA Proton Assignments. Nonexchangeable DNA protons were assigned using standard methods to identify sequential internucleotide dipolar connectivities (Figure 1). The assignments of the DNA proton resonances are tabulated in Table 1S in the supporting information. Except for the site of adduction, the internucleotide connectivities were characteristic of a B-type duplex. The NOESY connectivities through the adducted strand were disrupted by the presence of the aflatoxin lesion. While the T^4 H1′ → C^{5}H6 cross-peak was observed, no connectivity was observed between C^5 H1′ and ^{AFB}G^6 H8 in D_2O buffer. The latter resonance was observed at 9.17 ppm in H_2O buffer. The downfield shift was due to the positive charge on the imidazole ring of the modified guanine, which also increased the rate of exchange with solvent, rendering this proton resonance unobservable in the deuteriated buffer. In the complementary strand, the sequential NOE A^{16} H1′ → G^{17}H8 at the site across from the lesion was weak. However, it was observed in the NOESY experiment recorded at the longest mixing time (350 ms).

The assignments of the imino protons, except those of G^{11}, G^{21}, and ^{AFB}G^6, were successfully obtained on the basis of sequential connectivities between the imino protons of adjacent base pairs. These assignments are also found in Table 1S in the supporting information. The line widths of the terminal G^{11} and G^{21} imino protons and of the ^{AFB}G^6 imino proton were not sufficiently narrow to be successfully assigned from NOE connectivities. The remaining guanine imino assignments were confirmed by their respective NOEs to the cytosine H-bonded amino → cytosine non-H-bonded → cytosine H5 protons.

The adenine H2 protons were assigned on the basis of cross-strand NOEs to the thymine imino protons of the respective A·T base pairs. The assignment of A^{16} H2 was determined by its long-range connectivities with its own H1′ as well as the cross-strand connectivity to G^6 H1′. There was a significant upfield shift of this proton to 6.20 ppm. Confirmation of this assignment was accomplished by implementing a nonselective inversion recovery experiment. The H2 resonances of A^3, A^7, A^{13}, and A^{18} were readily identified between 7.7 and 8 ppm. Aflatoxin resonances AFB H6a and AFB H8 were also observed to have long T_1

[3] An alternative possibility is that d(CCATCGATCC)$_2$ forms a parallel-stranded structure and that the parallel-stranded structure exhibits the same reaction stoichiometry with aflatoxin epoxide.

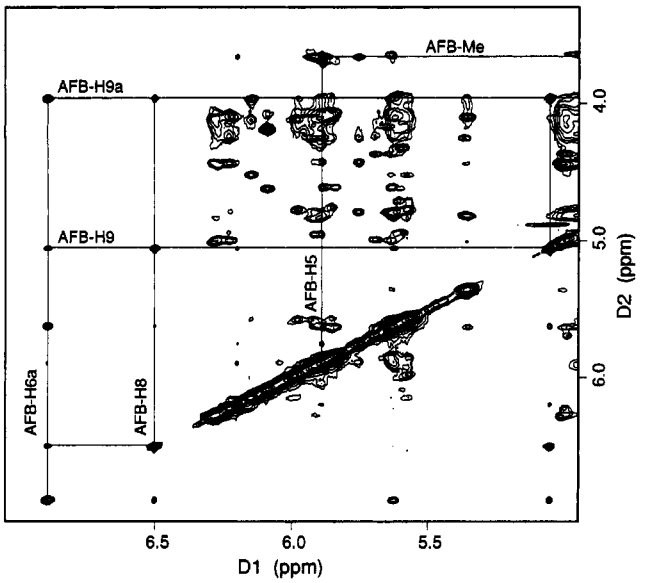

FIGURE 2: Connectivites of the aflatoxin B_1 furanose ring spin system and the H5 and the $-OCH_3$ protons at pD 6.9.

relaxation times. The slowly relaxing peak at 6.20 ppm was identified as A^{16} H2, in agreement with the observed H1′ connectivities.

(b) Aflatoxin Proton Assignments. Figure 2 shows the portion of the NOESY spectrum which displays the aflatoxin spin systems. The assignments of the AFB_1 ^1H resonances are collected in Table 2S in the supporting information. The connectivities between the furanose protons of aflatoxin, arising from AFB_1 H6a, H8, H9, and H9a, located these resonances at 6.89, 6.50, 5.05, and 3.96 ppm, respectively. The NOE between AFB_1 H5 and AFB_1 $-OCH_3$ located these resonances at 5.89 and 3.66 ppm. The methylene protons on the cyclopentenone ring were observed in the furthest upfield region of the spectrum, and they were partially superimposed with the deoxyribose H2′,H2″ protons as well as the thymine methyl protons (Figure 3).[4] The assignments of these protons were successfully accomplished on the basis of chemical shift (3α,β > 2α,β), previous NMR data of the aflatoxin adduct (Gopalakrishnan et al., 1990), NOE intensity patterns of the four methylene protons, and specific AFB−DNA NOEs to either the 5′-face α protons or the 3′-face β protons. Stronger cross-peaks were observed between the diastereotopic geminal protons at each position; weaker NOEs were observed between the vicinally coupled protons at each position.

NOEs between Aflatoxin and DNA Protons. A total of 43 NOEs were observed between aflatoxin and DNA protons. These are tabulated in Table 3S in the supporting information. AFB_1 H6a and H9a, the two protons located at the juncture of the fused furanose rings, showed a number of NOEs in the 5′-direction, particularly to C^5 of the C^5·G^{17} base pair. The H6a proton showed long-range NOEs to the methyl group on nucleotide T^4; these were presumed to have arisen from secondary effects due to spin diffusion in the NOESY experiments with longer mixing times. Both H6a and H9a exhibited NOEs to the imidazole proton of $^{AFB}G^6$, which were observed in experiments conducted in H_2O buffer. AFB_1 H8 and H9 exhibited cross-strand NOEs to A^{16} H2 and longer range (again, presumably secondary) NOEs to the 5′-neighbor base pair C^5·G^{17}. AFB_1 H5 and $-OCH_3$, located on the coumarin ring, exhibited a number of NOEs to the deoxyribose protons of C^5 and $^{AFB}G^6$. The methoxy protons also exhibited a cross-strand NOE to A^{16} H2. H2α,β of the aflatoxin cyclopentenone ring showed cross-strand NOE connectivities to A^{16} H1′ and to A^{16} H2. The AFB_1−DNA NOEs located the aflatoxin moiety on the 5′-face of the modified guanine ring, whereas the AFB_1−A^{16} connectivities located A^{16} within the helix. Figure 1A revealed the interesting observation that NOE connectivities characteristic of a B-form helix could be traced through the lesion site by incorporating aflatoxin−DNA NOEs. The 9.17 ppm resonance assigned to $^{AFB}G^6$ H8 exhibited NOEs to the H6a proton of the aflatoxin moiety as well as the expected intranucleotide NOE to $^{AFB}G^6$ H1′. The latter resonance showed the expected NOE to A^7 H8. Likewise, C^5 H6

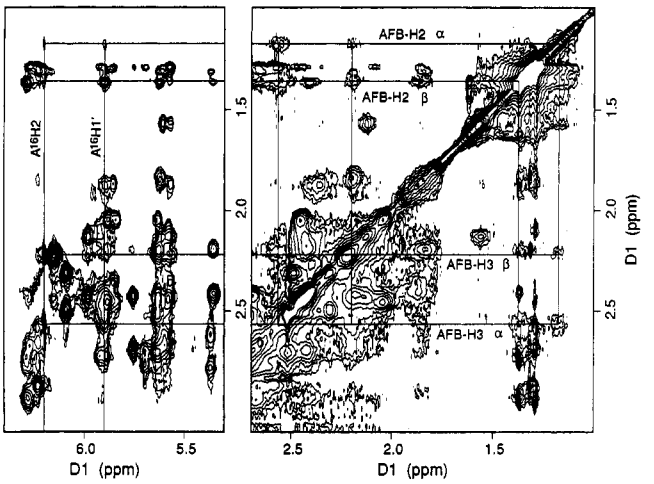

FIGURE 3: NOE connectivities between the methylenic H2 α,β and H3 α,β protons of aflatoxin B_1 and A^{16} H2 and A^{16} H1′ at pD 6.9.

Table 1: Distribution of NOE-Derived Distance Restraints, by Nucleotide

residue	intranucleotide	internucleotide	cross-strand non-H bonds
C^1	10	7	
C^2	6	14	
A^3	6	13	1
T^4	5	14	1
C^5	1	16	2
$^{AFB}G^6$	30	24	13
A^7	5	10	1
T^8	7	12	2
C^9	5	5	2
C^{10}	5	1	
G^{11}		1	
G^{12}	3	8	
A^{13}	6	13	4
T^{14}	8	15	1
C^{15}	11	12	
A^{16}	2	5	9
G^{17}	8	7	6
A^{18}	5	10	1
T^{19}	5	9	1
G^{20}	2	3	
G^{21}	9	1	

[4] The definitions of the enantiotopic protons at C2 and C3 are based upon the Cahn, Ingold, and Prelog nomenclature. We defined H2α to be the *pro-R* proton at C2; H2β is defined to be the *pro-S* proton at C2. H3α is defined to be the *pro-S* proton at C3, and H3β is defined to be the *pro-R* proton at C3. H2α and H3α lie on the same face of the cyclopentenone ring as do H6a and H9a; H2β and H3β lie on the other face of the cyclopentenone ring.

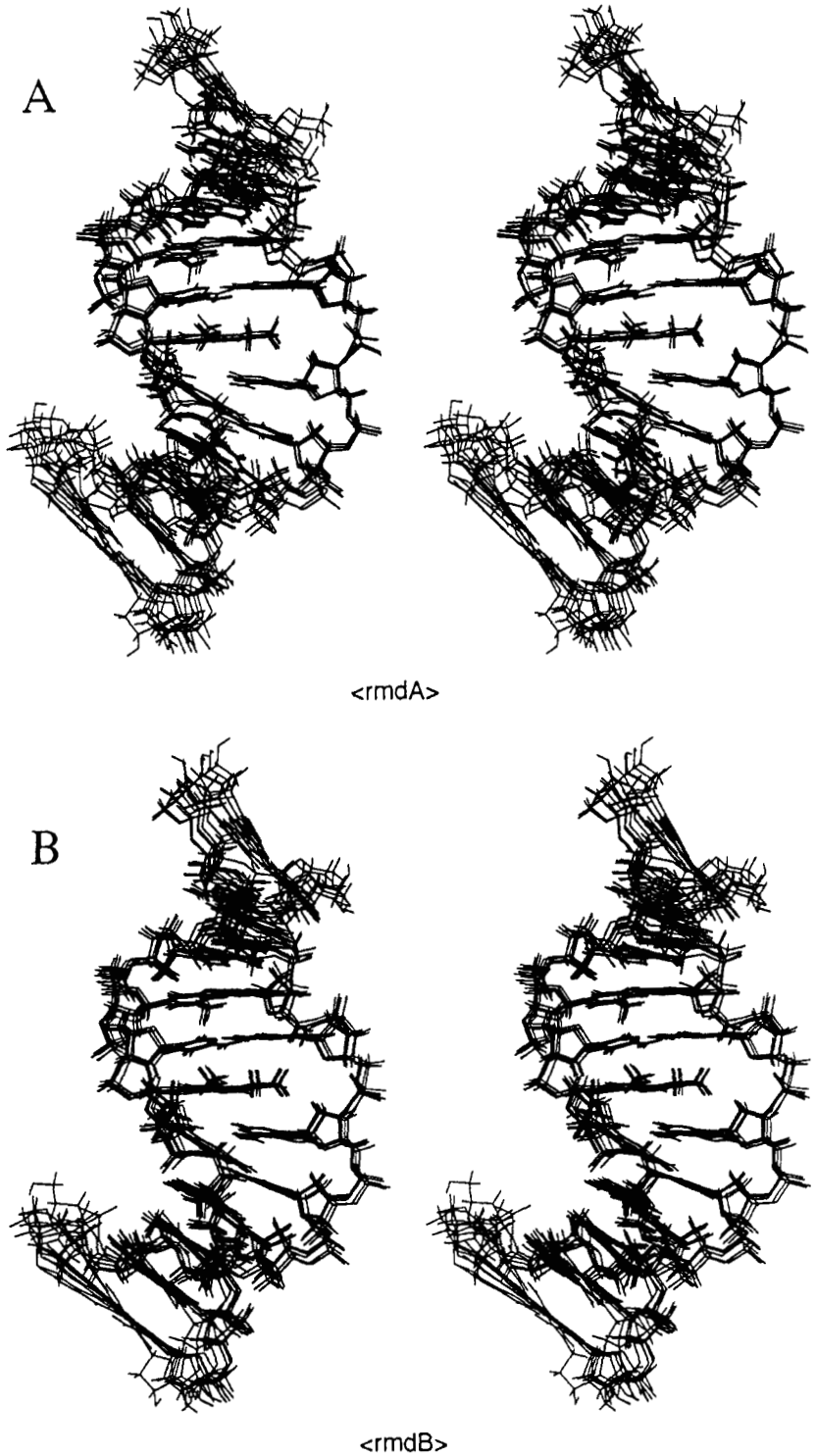

FIGURE 4: Stereo drawings of (A) six emergent MD structures calculated from IniB and (B) six emergent MD structures calculated from IniA.

exhibited an NOE to H6a of the aflatoxin moiety, thus allowing the sequential connectivities to be traced from C^5 to A^7 in the modified strand.

Structural Refinement. A breakdown of the type and distribution of 259 experimental and empirical distance constraints is given in Table 1. Six MD calculations were performed using different random seeds on both the IniA and IniB starting structures. Figure 4 superimposes the final MD structures from IniA and IniB in a stereoview presentation. Visual inspection of the overlayed structures revealed that the MD calculations, starting from either IniA or IniB, converged to a common structure, which was a right-handed helix. A final model shown in Figure 5 was arrived at by averaging these 12 structures followed by PEM. The calculations revealed that both the AFB_1 moiety and A^{16} were inserted into the DNA duplex. Figure 6 details the refined structure and resulting base stacking patterns at the adduct site.

The large number of NOEs observed between the aflatoxin moiety and the DNA enabled the site of the lesion to be well characterized. A total of 30 intranucleotide and 24 internucleotide NOEs were observed for $^{AFB}G^6$, as well as

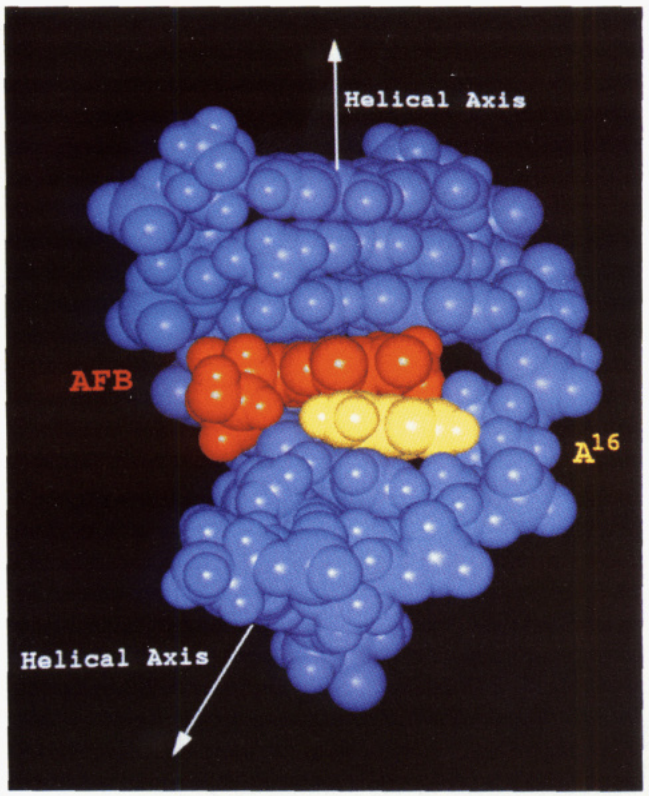

FIGURE 5: Final averaged structure from 12 calculated MD structures. The view is from the major groove.

13 cross-strand NOEs. The precision of the MD calculations was monitored by pairwise rms deviation between the emergent structures. Figure 7A shows that IniA and IniB were different, evidenced by rms deviations which generally were between 2 and 8 Å. Figure 7B,C revealed that the final averaged structure was different from either IniA or IniB. Figure 7D shows the convergence to the final averaged structure. The end base pairs were not well restrained. The average pairwise rms deviation for the entire molecule was 1.26 Å, while the rms deviation excluding terminal and penultimate base pairs was 0.85 Å. Back-calculation of the intensity matrix from the converged MD structures is summarized in Table 2. The sixth root *R*-factor R_1^x measured the difference between NOE intensities calculated by CORMA from the model structure and the intensities measured from the NOESY spectra (Keepers & James, 1984). Neither IniA nor IniB provided a satisfactory fit to the NOE data, although the value for R_1^x of 0.12 for IniB was somewhat better than the value of 0.16 for IniA. The R_1^x value decreased to 0.074 when the averaged MD structure was compared with the data, indicating satisfactory agreement between the refined structure and the NOE intensities.

Refined Structures. (a) Backbone Torsion Angles. The values from the IniA and IniB starting structures were calculated with reasonable precision and are displayed in Figure 8. A^{16}, the extra adenine in the complementary strand, was especially affected. For A^{16}, ϵ moved from the +ap range to the −ac range, ζ moved from −ac to −ap, α moved from −sc to +ap, and γ moved from +sc to +ap. At C^{15}, 3′ to the lesion site, α moved from −sc to +ap, while γ moved from +sc to +ap. At G^{17}, 5′ to the lesion site, α moved from −sc to −ac. Large deviations from canonical values were observed for angles α and γ at C^{10}, with smaller deviations observed in the remainder of the backbone angles at the terminal and penultimate nucleotides C^1, C^2, C^9, C^{10}, G^{11}, G^{12}, G^{20}, and G^{21}. There was no spectroscopic evidence to suggest unusual conformations at these nucleotides, although there was the usual evidence for terminal base-pair fraying, suggested by broadening and increased solvent-exchange rates for the imino protons on the terminal bases. These unusual helicoidal data were suspected to be due to an insufficient number of restraints. The calculated pseudorotation angles ϕ tended to be intermediate between the S and N deoxyribose conformations. Inspection of intensity patterns for $J_{H1',H2'}$ and $J_{H1',H2''}$ cross-peaks in a $^1H\{^{31}P\}$ DQF-COSY spectrum suggested that the deoxyribose rings were predominantly in the S conformation. The H2′ and H2″ of C^5 and A^{16} were not sufficiently resolved to evaluate their respective cross-peak intensity patterns in the COSY data.

(b) Intra-Base-Pair Helicoidal Parameters. Calculated values are shown in Figure 9. The MD calculations converged with good precision, beginning with either the IniA or IniB structures. The data for most of these parameters converged to values consistent with right-handed helices, but larger deviations were noticed for base-pair shearing, stagger, buckle, propeller twist, and opening. The calculations suggested that intercalation of the aflatoxin caused T^4·A^{18} and C^5·G^{17} to buckle away from the site of adduction. A large propeller twist was calculated for C^5·G^{17}. The existence of an opposing trend in the data on each side of the adduct was noted. Buckling, propeller twisting, stagger, shear, displacement, tip, and inclination all exhibited this effect to some degree. These results cannot be confirmed from the NMR data, and to some extent they may reflect an insufficient number of restraints in the MD calculations. The buckling of base pairs away from intercalation sites was observed in crystallographically determined intercalation complexes (Egli et al., 1991; Frederick et al., 1990).

(c) Inter-Base-Pair Helicoidal Parameters. The calculated values are shown in Figure 10. Each converged well from both IniA and IniB. With the exception of base pair step 5, corresponding to C^5·G^{17}→$^{AFB}G^6$·C^{15}, the inter-base-pair parameters tended to converge to values consistent with a right-handed B-like helix. The large deviations observed at base pair step 5 reflected the double intercalation of the aflatoxin moiety and A^{16} between base pairs C^5·G^{17} and $^{AFB}G^6$·C^{15}. Division of the base pair step 5 data by three, corresponding to the three intercalation steps C^5·G^{17}→AFB, AFB→A^{16}, and A^{16}→G^6·C^{15}, resulted in generation of the "average intercalation step value", denoted by the datum ×, indicated in all but the tilt plot of Figure 10. It was observed that the average intercalation step value tended to fall within the average deviation of shift, rise, and roll values calculated for the remainder of the molecule. For the slide parameter, it deviated from values calculated for the remainder of the molecule but still tended toward these values. The average intercalation step value measured for the twist parameter was indicative of the localized intercalation-induced unwinding of the helix at the site of the doubly intercalated aflatoxin moiety and A^{16}. The helical twist at the three intercalation steps C^5·G^{17}→AFB, AFB→A^{16}, and A^{16}→G^6·C^{15} was reduced to approximately 10°, as compared to the expectation value of ~34°. The calculated reduction in helical twist observed at base pair step 3 was believed to be artifactual, resulting from insufficient restraints in the MD calculations.

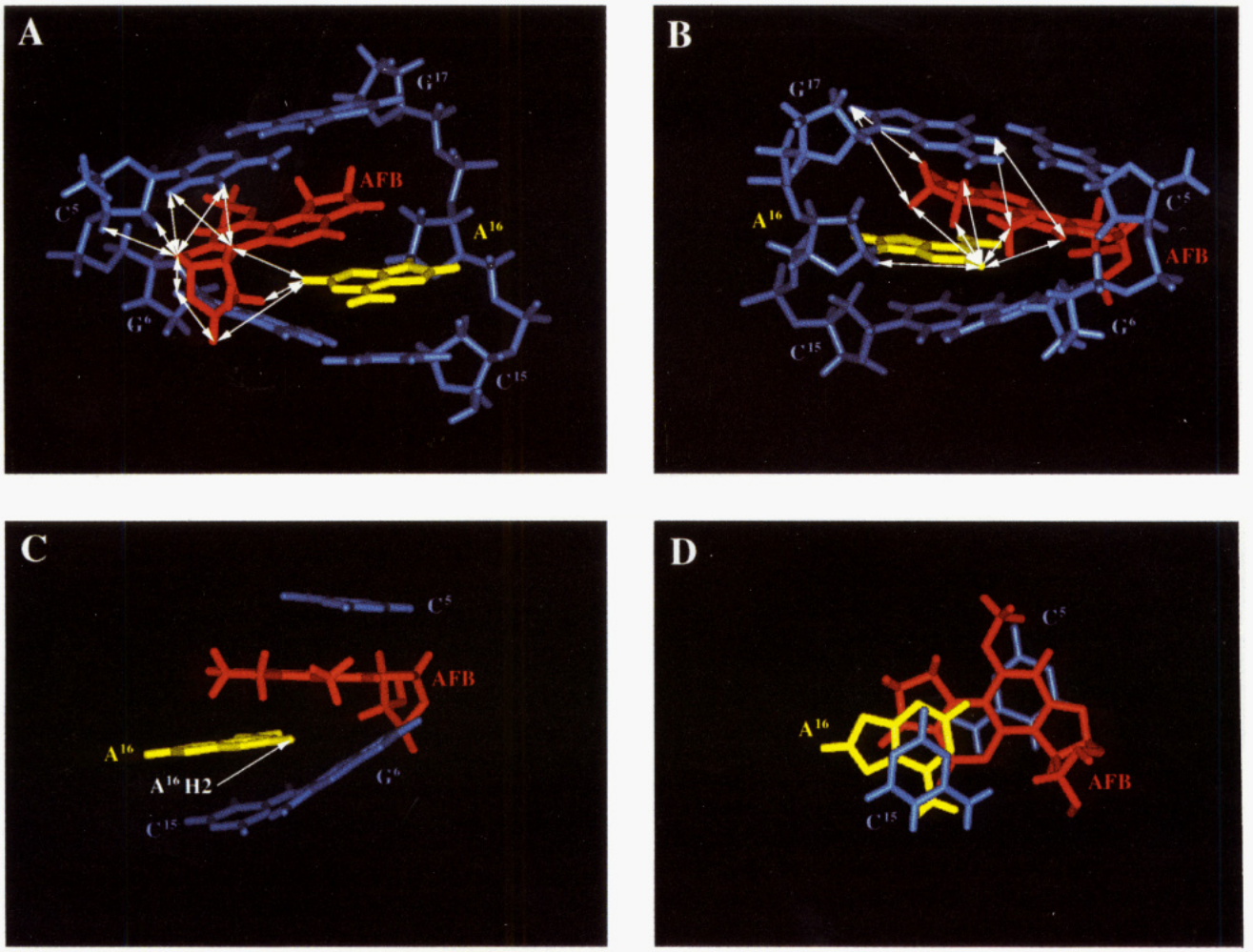

FIGURE 6: View of the aflatoxin moiety from (A) the major groove and (B) the minor groove. The arrows represent observed NOEs which were used in MD calculations. The AFB_1 furanose ring NOEs are seen from the major groove. The H5, $-OCH_3$, and the AFB_1 methylene protons lie in the minor groove, and hence those NOEs are shown from that perspective. Stacking interactions (C) as seen in an edgewise view from the minor groove and (D) as seen perpendicular to the helix axis.

DISCUSSION

Aflatoxin B_1, a mycotoxin and a strong environmental mutagen, is of concern due to its frequent contamination of a variety of economically important agricultural products. Random mutagenesis studies demonstrated base substitutions, especially G → T transversions, to be the predominant mutations induced by aflatoxin B_1 (Foster et al., 1983, 1988; McMahon et al., 1990; Bressac et al., 1991; Hsu et al., 1991; Levy et al., 1992; Trottier et al., 1992). Lower levels of frame shifts were also documented (Refolo et al., 1987; Sambamurti et al., 1988; Bennett et al., 1991). Structural studies demonstrated that two cationic adducts of AFB_1, d(ATC^{AFB}GAT)·d(ATCGAT) and $d(ATGCAT)_2$, were intercalated above the 5′-face of the modified guanines (Gopalakrishnan et al., 1990). An adduct of sterigmatocystin was intercalated in a similar manner (Gopalakrishnan et al., 1992). These structures predicted that, functionally, aflatoxin adducts might induce mutations at the lesion site or in the 5′-direction from the lesion site. The long-range goal of this work is to understand how aflatoxin intercalation might induce specific mutations.

Adduct Conformation opposite an Extra Adenine. At pD 6.9 the aflatoxin moiety remained intercalated above the 5′-face of the modified guanine in d(CCATC^{AFB}GATCC)·d(GGATCAGATGG), in an orientation similar to that previously observed for d(ATC^{AFB}GAT)·d(ATCGAT), when no extra base was incorporated opposite aflatoxin (Gopalakrishnan et al., 1990). The extra adenine incorporated opposite the aflatoxin moiety in the complemenatary strand (A^{16}) is also inserted into the DNA duplex. These interactions, in which the aflatoxin moiety stacks beneath base pair C^5·G^{17}, and A^{16} stacks between the aflatoxin moiety and base pair $^{AFB}G^6$·C^{15}, are shown in Figure 6C,D. The structure containing an extra adenine opposite the modified guanine was found to be more energetically stable than would be the case if an extra adenine base were present in the complementary strand of the duplex at that position.

Several lines of evidence support the above conclusions. A total of 43 DNA−aflatoxin cross-peaks, many of which are represented schematically in Figure 6A,B, provided a pattern of NOEs consistent with both the aflatoxin moiety and A^{16} being intercalated. NOEs were observed from the AFB_1 H6a and H9a to C^5 H5 and H6, located in the 5′-direction from the site of adduction. The magnitude of the NOE between A^{16} H8 and A^{16} H1′ confirmed that A^{16} is in the *anti* conformation about the glycosyl bond. A disturbance of the sugar backbone was evidenced by the very weak NOE between A^{16} H1′ and G^{17} H8 at 350 ms mixing time, which resulted in a greater than normal calculated distance between these two protons. However, additional NOEs to

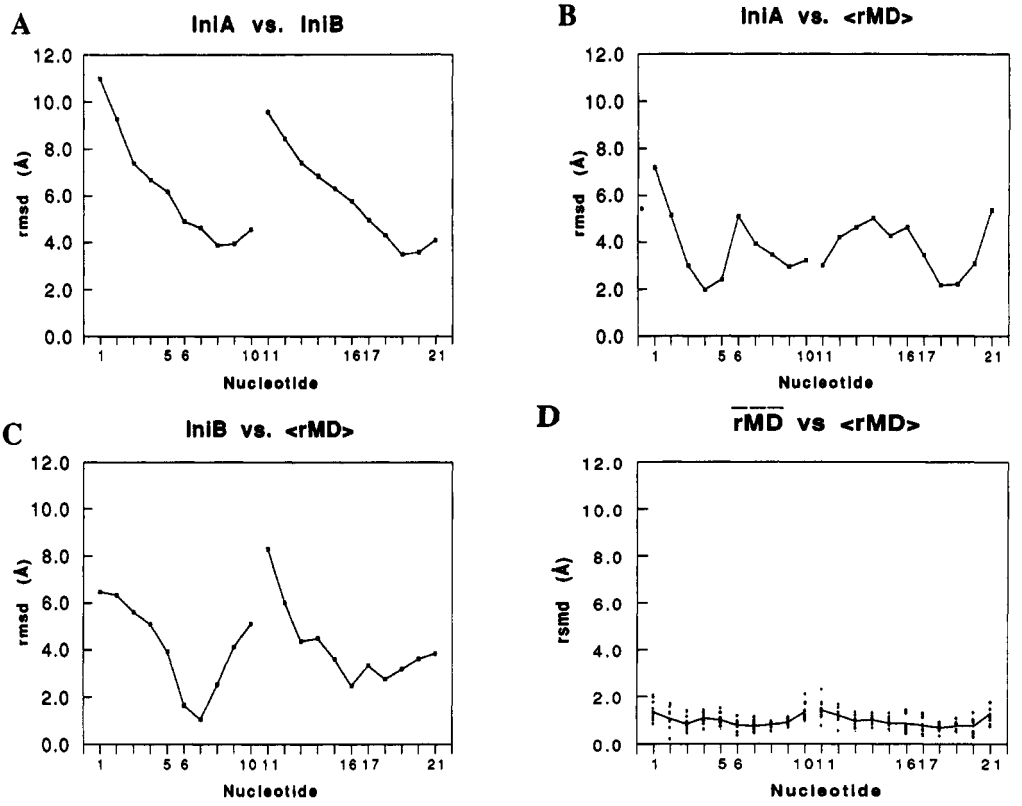

FIGURE 7: The rms differences in angstroms (A) between IniA and IniB, (B) between IniA and the final average MD structure, (C) between IniB and the final average MD structure, and (D) between each of the 12 MD structures and the final averaged MD structure. In (D) the 12 structures are shown as a spread of rms deviation/base, and the average rms deviation is given by the solid line.

Table 2: Comparison of Sixth Root Residual Indices R_1^x for Starting Models and MD Structures[a]

	R_1^x		
structure	150 ms	250 ms	350 ms
IniA		16×10^{-2}	
IniB		12×10^{-2}	
rMDA	8.87×10^{-2}	7.57×10^{-2}	7.22×10^{-2}
rMDB	8.43×10^{-2}	7.43×10^{-2}	7.00×10^{-2}
rMD_{final}	8.20×10^{-2}	7.28×10^{-2}	6.90×10^{-2}

[a] The terminal base pairs were not included in the calculations to exclude end effects. $R_1^x = \sum|(a_o)_i^{1/6} - (a_c)_i^{1/6}|/\sum|(a_o)_i^{1/6}|$, where a_o and a_c are the intensities of observed (non-zero) and calculated NOE cross-peaks. IniA, starting energy-minimized A-DNA; IniB, starting energy-minimized B-DNA; rMDA, average of 6 rMD structures starting from IniA; rMDB, average of 6 rMD structures starting from IniB; rMD_{final}, average of 12 rMD structures starting from IniA and IniB.

A^{16} (Figure 6B), especially those between the AFB_1 $H2_{\alpha,\beta}$, $H3_{\alpha,\beta}$, and G^6 H1′ with A^{16} H2, confirm that this nucleotide is stacked into the double helix. The aflatoxin−DNA NOEs extend the standard sequential NOE connectivities observed for B-type DNA through the aflatoxin moiety (Figure 1B). Chemical shift changes are also consistent with both the aflatoxin moiety and A^{16} being intercalated into the helix. The chemical shifts of the aflatoxin protons are similar to those observed for d(ATC^{AFB}GAT)·d(ATCGAT) (Gopalakrishnan et al., 1990). In addition, the unusual upfield shift of A^{16} H2 strongly suggests an intercalated position for this proton. Inspection of the rMD structures reveals that A^{16} H2 is stacked just above the aromatic ring of $^{AFB}G^6$ and below the coumarin ring of the aflatoxin (Figure 6B,C).

A prominent feature of the MD structures is a localized adduct-induced bend at the lesion site (Figure 5). The bend separates the molecule into two domains. The top domain consists of C^1·G^{21}, C^2·G^{20}, A^3·T^{19}, T^4·A^{18}, and C^5·G^{17}. The aflatoxin moiety of $^{AFB}G^6$ stacks below the top domain. The bottom domain consists of $^{AFB}G^6$·C^{15}, A^7·T^{14}, T^8·A^{13}, C^9·G^{12}, and C^{10}·G^{11}. The bend is induced by the 36° angle between the plane of $^{AFB}G^6$·C^{15} and the plane of the aflatoxin moiety, which is required by sp^2 geometry at N7 of $^{AFB}G^6$ (see discussion below). The MD calculations suggest that the backbone torsion angles α (P→O5′) and γ (C5′→C4′) of A^{16} and G^{17} shift from the −sc to the ap range, accommodating the bend in the duplex at the adduct site. The ε (C3′→O3′) angle is also calculated to be somewhat increased at A^{16} and decreased at G^{17}. These calculated torsion angle perturbations are oriented in the 5′-direction from $^{AFB}G^6$, consistent with intercalation of the AFB moiety above the 5′-face of this nucleotide. The resulting wedge in the DNA structure enables the aromatic ring of A^{16} to fit between the AFB_1 ring and C^{15}·$^{AFB}G^6$. The weak NOE between A^{16} H8 and G^{17} H8 is consistent with the greater than normal distance between these protons. This is likely a secondary (spin diffusion) NOE transferred via the methylenic protons of the aflatoxin moiety. The calculations suggest that intercalation of the aflatoxin causes T^4·A^{18} and C^5·G^{17} to buckle away from the site of adduction (Figure 9), similar to what has been observed in crystallographically determined intercalation structures (Egli et al., 1991; Frederick et al., 1990).

Unwinding. A second feature of the refined structures is the localized unwinding of the DNA duplex. Unwinding is expected in light of the observation that d(CCATC^{AFB}-GATCC)·d(GGATCAGATGG) forms a doubly intercalated complex, with both aflatoxin and A^{16} inserted into the helix. Figure 10 shows that the average winding angle between C^5·G^{17}, the intercalated aflatoxin moiety, A^{16}, and $^{AFB}G^6$·C^{15} is ~10°, as compared to the canonical value of 34°. The

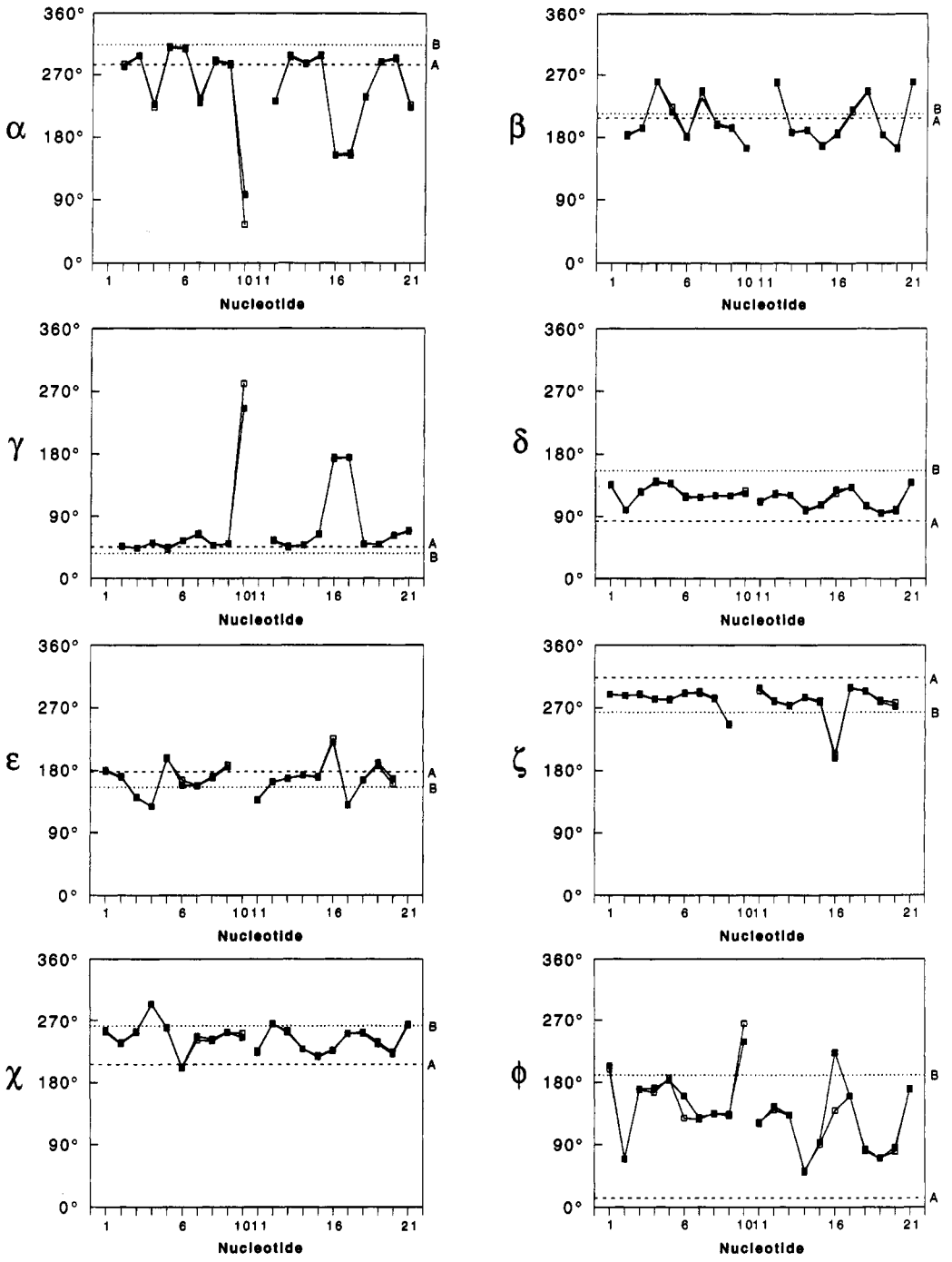

FIGURE 8: Phosphodiester backbone torsion angles for the IniA and IniB sets of structures. A- and B-DNA values are shown as the dashed and dotted lines, respectively.

NOE data from ^{1}H NMR cannot confirm the presence of bending and unwinding of the DNA at the adduct site. However, the observation that neither IniA or IniB agrees well with the refined MD structures is consistent with the induction of adduct-induced bending and unwinding of the helix. Chemical shift perturbations observed in ^{31}P NMR data (not shown) suggested adduct-induced changes in the backbone which would corroborate the refined structures.

pH Dependence. The potential formation of a pseudo-base-pair between the aflatoxin moiety and A[16] requires protonation of the latter at N1 and hence should impart a pH dependence to the conformation of this adduct. The themodynamic data did reveal an increased stability for the duplex at lower pH. However, a ^{1}H NMR spectrum obtained at lower pH revealed no evidence of hydrogen bonding involving the aflatoxin and A[16].[5] This perhaps argues that, for this interaction, the favorable free energy of base-stacking interactions is greater than the free energy obtained by forming a pseudo-base-pairing interaction between aflatoxin and adenine. There may also be a reduction in the steric strain imposed upon the molecule when the adenine is stacked, as opposed to a base-pairing interaction of two large moieties in the intrahelical area of the duplex.

Hybridization at Guanine N7. Formation of the cationic N7 adduct of AFB_1 places a positive charge on the imidazole

[5] It is possible that rapid exchange with solvent precludes observation of hydrogen bonding between aflatoxin and adenine at the lower pH. Base pairing involving protonated adenine has proved difficult to observe in other instances.

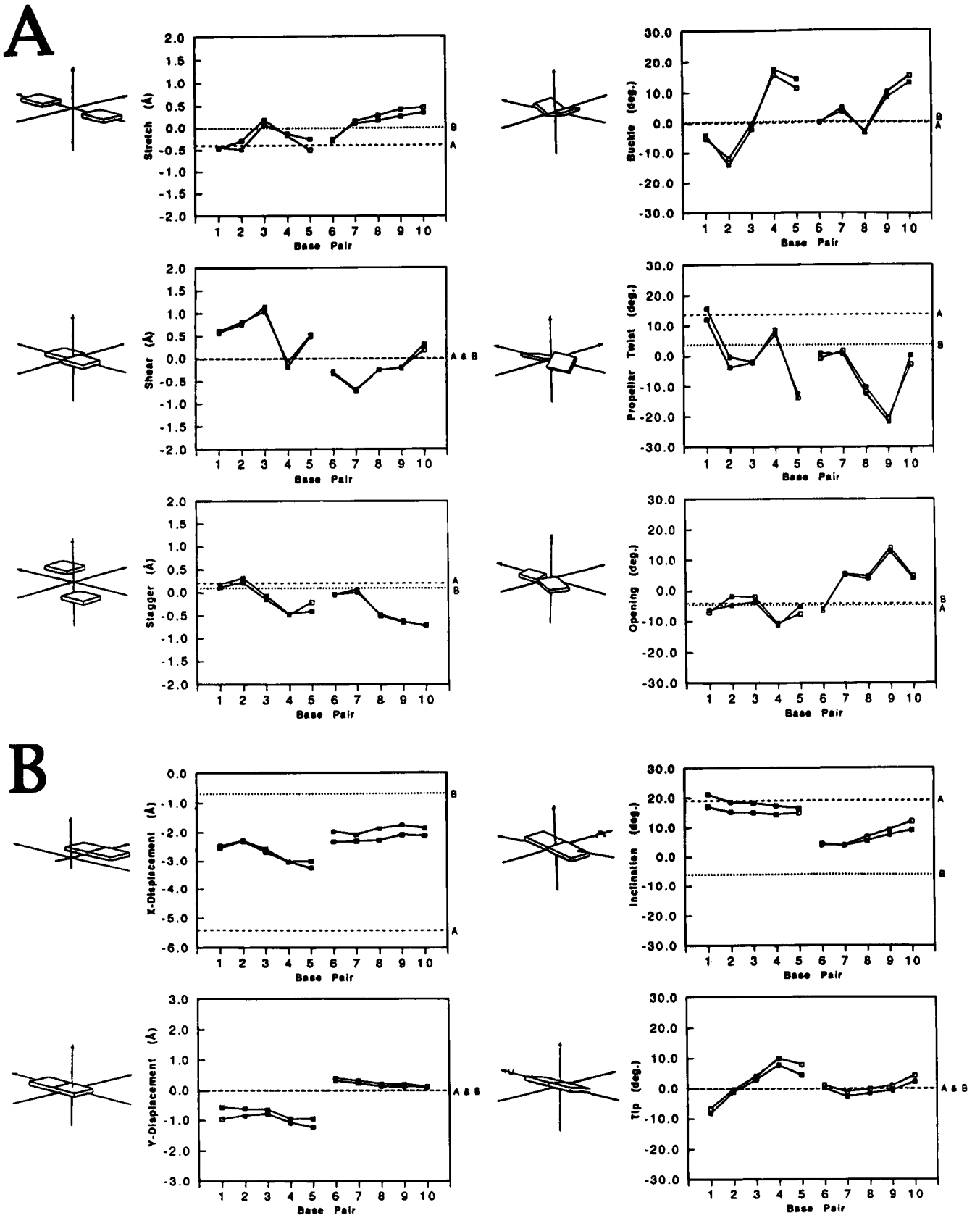

FIGURE 9: Intra-base-pair parameters for the IniA and IniB sets of structures. A- and B-DNA values are shown as the dashed and dotted lines, respectively. The base-pair numbering scheme in the figure is based on the adducted strand; i.e., base pair 7 corresponds to A^7·T^{14}. (A) Parameters relating to the position of the two nucleotides comprising each base pair. (B) Calculated values relating to the position of each base pair with respect to the helical axis.

ring of the modified guanine. A previous study of a sterigmatocystin−oligodeoxynucleotide adduct hybridized guanine N7 as sp^3 in PEM calculations, thus localizing the adduct-induced positive charge (Gopalakrishnan et al., 1992). The PEM calculations predicted a lower energy for the sp^3- versus the sp^2-hybridized adduct (Gopalakrishnan et al.,

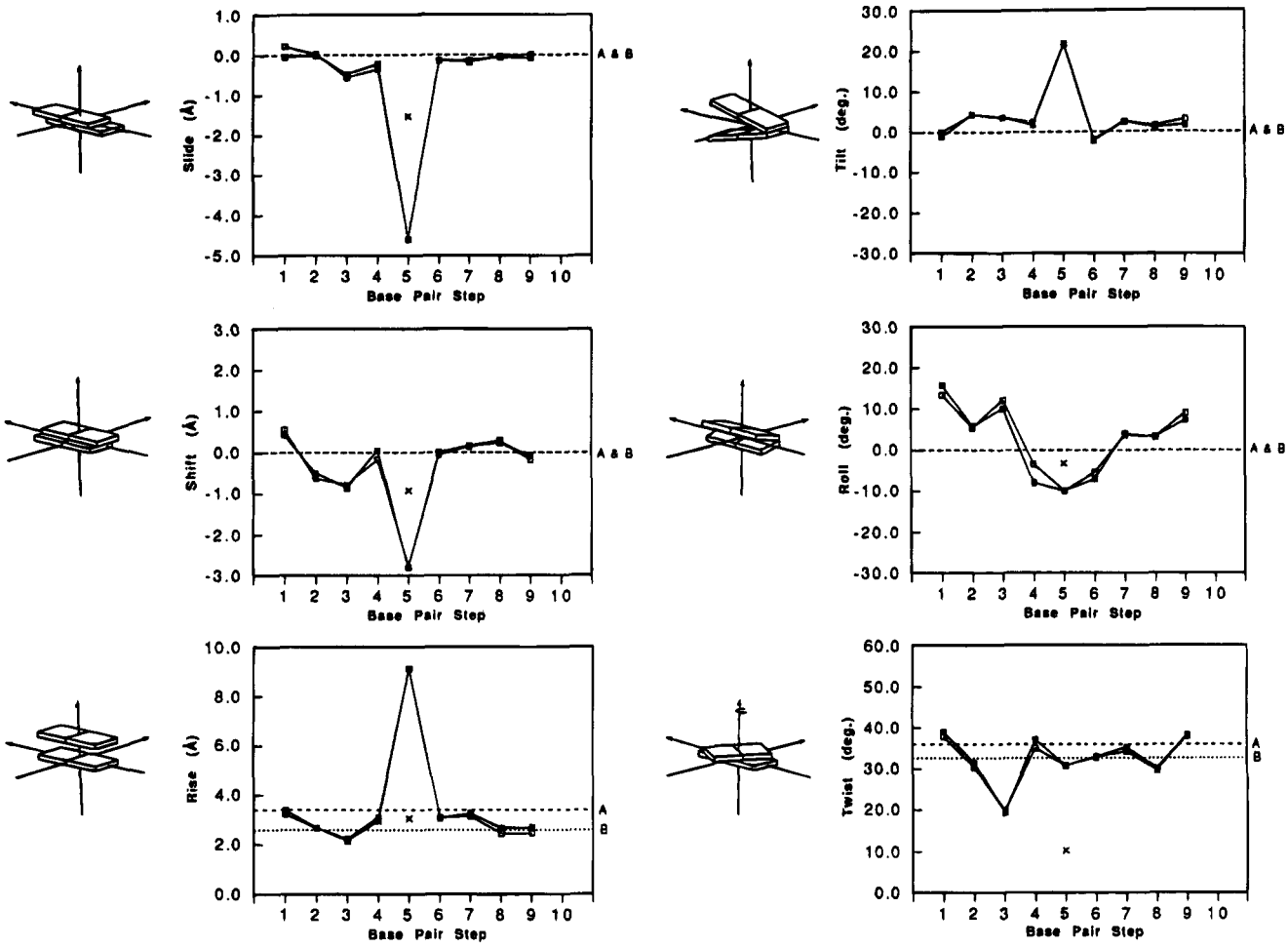

FIGURE 10: Inter-base-pair parameters for the IniA and IniB sets of structures. A- and B-DNA values are shown as the dashed and dotted lines, respectively. The base-step numbering scheme is based upon the adducted strand; i.e., base step 7 corresponds to d(A^7→T^8)·d(A^{13}→T^{14}). Values for the base step through the adduct, C^5·G^{17}→$^{AFB}G^6$·C^{15}, were measured only on the final averaged structure. The datum × indicates the "average intercalation step value" at the site of the adduct.

1992). The change from sp^2 to sp^3 hybridization at guanine N7 imparts a significant difference to the refined solution structure of the molecule, which might account for the observed difference in energies. If sp^3 hybridization is invoked, the aflatoxin moiety can stack into the DNA duplex with minimal structural perturbation and no induced bending (Gopalakrishnan et al., 1992). Intercalation from sp^2 hybridization requires adduct-induced bending of the DNA at the lesion site.

We elected to maintain sp^2 hybridization at $^{AFB}G^6$ N7. In this work, the stacking of A^{16} between the aromatic rings of AFB_1 and of the modified guanine to create a wedge-like perturbation at the lesion site was consistent with sp^2 but not sp^3 hybridization. In the latter case, the aflatoxin moiety would be parallel to the modified guanine. Stacking the A^{16} purine ring between the guanine and aflatoxin moieties in $^{AFB}G^6$ would violate van der Waals restraints between the two ring systems. SCF calculations assuming sp^2 hybridization for N7 predicted the positive charge to be distributed in both the imidazole ring of the modified guanine and the terminal furan ring of the aflatoxin moiety (Pullman & Pullman, 1986; Renugopalakrishnan et al., 1971) (Figure 1S in the supporting information).

The higher potential energy of the sp^2-hybridized as compared to the sp^3-hybridized structure could be consistent with the chemical instability of this adduct, which undergoes depurination and converts to the ring-opened FAPY derivative under basic conditions. Facile rearrangement to the FAPY derivative was not observed in the case of a non-intercalating N7 lesion, which did not create steric obstruction to the DNA duplex (Humphreys et al., 1990). Indirect evidence argues in favor of sp^2 hybridization at guanine N7. Formation of the cationic *trans*-8,9-dihydro-8-(*N*^{7}-guanyl)-9-hydroxyaflatoxin B_1 adduct results in line broadening concomitant with a downfield shift of $^{AFB}G^6$ N1H (Gopalakrishnan et al., 1990), consistent with the notion that the positive charge has been delocalized.

Structure–Function Considerations. The aflatoxin B_1 adduct opposite CpA in the complementary strand models a structure which potentially leads to a +1 addition mutation. The adenine opposite the cationic aflatoxin moiety does not cause major disruption of the DNA helix and is thermodynamically favorable, as compared to the insertion of an extra adenine in the corresponding unmodified duplex. One might speculate that this adduct templates +1 additions. However, such mutations have not been extensively reported in random mutagenesis studies of aflatoxin B_1. Most studies have shown AFB_1 to be mainly a base substitution mutagen, inducing predominantly G → T transversions (*vide ante*). We conclude that thermodynamic stability of this structure *per se* does not reliably predict +1 frame shifts. Whether cationic aflatoxin adducts result in low levels of templated

additions 5′ to lesion sites *in vivo*, in addition to G → T transversions, is not known. In some systems with high sensitivity to frame-shift detection, it has been shown that frame shifts occur at low frequency. For example, aflatoxins are active in frame-shift-sensitive tester strains of *Salmonella typhimurium* (McCann et al., 1975), and frame shifts are observed in random mutagenesis studies (Refolo et al., 1987; Sambamurti et al., 1988; Bennett et al., 1991). Site-directed DNA replication (Shibutani et al., 1991) and mutagenesis (Loechler et al., 1984; Green et al., 1984) studies should help to determine whether templated +1 additions represent a minor mutagenesis pathway for cationic aflatoxin B_1 lesions. Minor components of the mutational spectrum could be important, since the biological significance of specific events is expected to correlate with their occurrences in crucial genetic loci, such as coding regions for the active sites of DNA repair genes, protooncogenes, or tumor suppressor genes.

ACKNOWLEDGMENT

Dr. Rajkumar S. Iyer assisted with the synthesis of aflatoxin B_1 *exo*-8,9-epoxide, Professors Thomas M. Harris and Carmelo J. Rizzo were consulted regarding aflatoxin chemistry, Dr. Irene Zegar and Mr. Markus Voehler assisted with acquisition of NMR spectra, Mr. Jason P. Weisenseel assisted with the structural refinement, and Ms. Jacqueline Johnston and Ms. Randi Tinkham assisted in preparing the manuscript.

SUPPORTING INFORMATION AVAILABLE

A detailed description of the empirical restraints used in the MD protocol and a description of the protocol itself (2 pages), resonance assignments of d(CCATC^{AFB}GATCC)·d(GGATCAGATGG) (1 table), resonance assignments of the aflatoxin B_1 moiety (1 table), NOEs observed between aflatoxin B_1 protons and DNA protons (1 table), NOE restraints used in the MD calculations (4 tables), partial charges of 8,9-*trans*-dihydro-8-(N^7-guanyl)-9-hydroxy-aflatoxin B_1 (1 figure), and melting data for d(CCATC^{AFB}GATCC)·d(GGATCAGATGG) and related oligodeoxynucleotides (1 figure) (15 pages). Ordering information is given on any current masthead page.

REFERENCES

Aoyama, T., Yamano, S., Guzelian, P. S., Gelboin, H. V., & Gonzalez, F. J. (1990) *Proc. Natl. Acad. Sci. U.S.A. 87*, 4790−4793.

Arnott, S., & Hukins, D. W. L. (1972) *Biochem. Biophys. Res. Commun. 47*, 1504−1509.

Arnott, S., & Hukins, D. W. L. (1973) *J. Mol. Biol. 81*, 93−105.

Baertschi, S. W., Raney, K. D., Stone, M. P., & Harris, T. M. (1988) *J. Am. Chem. Soc. 110*, 7929−7931.

Bax, A., Sklenar, V., & Clore, G. M. (1987) *J. Am. Chem. Soc. 109*, 6511−6513.

Bennett, C. B., Luo, X., & Humayun, M. Z. (1991) *Mutat. Res. 249*, 19−27.

Berendsen, H. J. C., Postma, J. P. M., van Gunsteren, W. F., DiNola, A., & Haak, J. R. (1984) *J. Phys. Chem. 81*, 3684−3690.

Bodenhausen, G., Wagner, G., Rance, M., Sorensen, O. W., Wuthrich, K., & Ernst, R. R. (1984) *J. Magn. Reson. 59*, 542−550.

Borer, P. N. (1975) in *Handbook of Biochemistry and Molecular Biology*, CRC Press, Cleveland OH.

Borgias, B. A., & James, T. L. (1990) *J. Magn. Reson. 87*, 475−487.

Bressac, B., Kew, M., Wands, J., & Ozturk, M. (1991) *Nature 350*, 429−431.

Brooks, B. R., Bruccoleri, R. E., Olafson, B. D., States, D. J., Swaminathan, S., & Karplus, M. (1983) *J. Comput. Chem. 4*, 187−217.

Brunger, A. T. (1992) in *X-PLOR. Version 3.1. A System for X-ray Crystallography and NMR*, Yale University Press, New Haven, CT.

Busby, W. F., Jr., & Wogan, G. N. (1984) in *Chemical Carcinogens* (Searle, C. E., Ed.) pp 945−1136, American Chemical Society, Washington, DC.

Clore, G. M., Gronenborn, A. M., Carlson, G., & Meyer, E. F. (1986) *J. Mol. Biol. 190*, 259−267.

Egli, M., Williams, L. D., Frederick, C. A., & Rich, A. (1991) *Biochemistry 30*, 1364−1372.

El-Dessouki, S. (1992) *Food Chem. Toxicol. 30*, 993−994.

Essigmann, J. M., Croy, R. G., Nadzan, A. M., Busby, W. F., Jr., Reinhold, V. N., Buchi, G., & Wogan, G. N. (1977) *Proc. Natl. Acad. Sci. U.S.A. 74*, 1870−1874.

Foster, P. L., Eisenstadt, E., & Miller, J. H. (1983) *Proc. Natl. Acad. Sci. U.S.A. 80*, 2695−2698.

Foster, P. L., Groopman, J. D., & Eisenstadt, E. (1988) *J. Bacteriol. 170*, 3415−3420.

Frederick, C. A., Williams, L. D., Ughetto, G., Van Der Marel, G. A., Van Boom, J. H., Rich, A., & Wang, A. H.-J. (1990) *Biochemistry 29*, 2538−2549.

Gopalakrishnan, S., Byrd, S., Stone, M. P., & Harris, T. M. (1989a) *Biochemistry 28*, 726−734.

Gopalakrishnan, S., Stone, M. P., & Harris, T. M. (1989b) *J. Am. Chem. Soc. 111*, 7232−7239.

Gopalakrishnan, S., Harris, T. M., & Stone, M. P. (1990) *Biochemistry 29*, 10438−10448.

Gopalakrishnan, S., Liu, X., & Patel, D. J. (1992) *Biochemistry 31*, 10790−10801.

Green, C. L., Loechler, E. L., Fowler, K. W., & Essigmann, J. M. (1984) *Proc. Natl. Acad. Sci. U.S.A. 81*, 13−17.

Groopman, J. D., Cain, L. G., & Kensler, T. W. (1988) *CRC Crit. Rev. Toxicol. 19*, 113−145.

Hore, P. J. (1983) *J. Magn. Reson. 54*, 539−542.

Hsu, I. C., Metcalf, R. A., Sun, T., Welsh, J. A., Wang, N. J., & Harris, C. C. (1991) *Nature 350*, 427−428.

Humphreys, W. G., Kim, D. H., Cmarik, J. L., Shimada, T., & Guengerich, F. P. (1990) *Biochemistry 29*, 10342−10350.

Iyer, R., & Harris, T. M. (1993) *Chem. Res. Toxicol. 6*, 313−316.

Iyer, R. S., Coles, B. F., Raney, K. D., Thier, R., Guengerich, F. P., & Harris, T. M. (1994) *J. Am. Chem. Soc. 116*, 1603−1609.

James, T. L. (1991) *Curr. Opin. Struct. Biol. 1*, 1042−1053.

Keepers, J. W., & James, T. L. (1984) *J. Magn. Reson. 57*, 404−426.

Levy, D. D., Groopman, J. D., Lim, S. E., Seidman, M. M., & Kraemer, K. H. (1992) *Cancer Res. 52*, 5668−5673.

Loechler, E. L., Green, C. L., & Essigmann, J. M. (1984) *Proc. Natl. Acad. Sci. U.S.A. 81*, 6271−6275.

Macura, S., Wuthrich, K., & Ernst, R. R. (1982) *J. Magn. Reson. 47*, 351−357.

Marion, D., Ikura, M., & Bax, A. (1989) *J. Magn. Reson. 84*, 425−430.

McCann, J., Spingain, N. E., Ikobori, J., & Ames, B. N. (1975) *Proc. Natl. Acad. Sci. U.S.A. 72*, 979−983.

McMahon, G., Davis, E. F., Huber, L. J., Kim, Y., & Wogan, G. N. (1990) *Proc. Natl. Acad. Sci. U.S.A. 87*, 1104−1108.

Murray, R. W., & Jeyaraman, R. (1985) *J. Org. Chem. 50*, 2847−2853.

Nilsson, L., & Karplus, M. (1986) *J. Comput. Chem. 7*, 591−616.

Plateau, P., & Gueron, M. (1982) *J. Am. Chem. Soc. 104*, 7310−7311.

Pullman, A., & Pullman, B. (1986) *Adv. Quantum Chem. 4*, 267−325.

Rance, M., Bodenhausen, G., Wagner, G., Wuthrich, K., & Ernst, R. R. (1985) *J. Magn. Reson. 62*, 497−510.

Raney, K. D., Gopalakrishnan, S., Byrd, S., Stone, M. P., & Harris, T. M. (1990) *Chem. Res. Toxicol. 3*, 254−261.

Raney, V. M., Harris, T. M., & Stone, M. P. (1993) *Chem. Res. Toxicol. 6*, 64−68.

Ravishankar, G., Swaminathan, S., Beveridge, D. L., Lavery, R., & Sklenar, H. (1989) *J. Biomol. Struct. Dyn. 6*, 669−699.

Refolo, L. M., Bennett, C. B., & Humayun, M. Z. (1987) *J. Mol. Biol. 193*, 609−636.

Renugopalakrishnan, V., Lakshminarayanan, A. V., & Sasisekharan, V. (1971) *Biopolymers 10*, 1159−1167.

Ryckaert, J.-P., Ciccotti, G., & Berendsen, H. J. C. (1977) *J. Comput. Phys. 23*, 327−341.

Sambamurti, K., Callahan, J., Luo, X., Perkins, C. P., Jacobsen, J. S., & Humayun, M. Z. (1988) *Genetics 120*, 863−873.

Shibutani, S., Takeshita, M., & Grollman, A. P. (1991) *Nature 349*, 431−434.

Shimada, T., & Guengerich, F. P. (1989) *Proc. Natl. Acad. Sci. U.S.A. 86*, 462−465.

Sklenar, V., Brooks, B. R., Zon, G., & Bax, A. (1987) *FEBS Lett. 216*, 249−252.

Soman, N. R., & Wogan, G. N. (1993) *Proc. Natl. Acad. Sci. U.S.A. 90*, 2045−2049.

Stewart, J. P. (1983) *Quantum Chem. Prog. Bull. 3*, 43.

Stone, M. P., Gopalakrishnan, S., Harris, T. M., & Graves, D. E. (1988) *J. Biomol. Struct. Dyn. 5*, 1025−1041.

Stone, M. P., Gopalakrishnan, S., Raney, K. D., Raney, V. M., Byrd, S., & Harris, T.M. (1990) in *Molecular Basis of Specificity in Nucleic Acid−Drug Interactions* (Pullman, B., & Jortner, J., Eds.) pp 451−480, Kluwer Academic Publishers, Dordrecht, The Netherlands.

Trottier, Y., Waithe, W. I., & Anderson, A. (1992) *Mol. Carcinog. 6*, 140−147.

Van Soest, T. C., & Peerdeman, A. F. (1970) *Acta Crystallogr. B26*, 1940−1963.

Wogan, G. N. (1992) *Prog. Clin. Biol. Res. 374*, 123−137.

BI9429748